Optics Letters

Coherence properties of a 2.6–7.5 μm frequency comb produced as a subharmonic of a Tm-fiber laser

V. O. Smolski,[1,2] H. Yang,[3] S. D. Gorelov,[4] P. G. Schunemann,[5] and K. L. Vodopyanov[1,*]

[1]CREOL, College of Optics and Photonics, University of Central Florida, Orlando, Florida 32816, USA
[2]IPG Photonics—Mid-Infrared Lasers, Birmingham, Alabama 35203, USA
[3]Department of Precision Instruments, Tsinghua University, Beijing 100084, China
[4]University of Nizhny Novgorod, Nizhny Novgorod 603950, Russia
[5]BAE Systems, P.O. Box 868, MER15-1813, Nashua, New Hampshire 03061, USA
*Corresponding author: vodopyanov@creol.ucf.edu

Received 21 January 2016; revised 20 February 2016; accepted 23 February 2016; posted 24 February 2016 (Doc. ID 257200); published 17 March 2016

We study the temporal coherence of an ultrabroadband frequency comb produced in a degenerate GaAs optical parametric oscillator (OPO) pumped by a stabilized Tm-fiber comb, by observing multiheterodyne beats in the RF domain. We infer that in such a regime the OPO automatically produces a stable frequency comb that is phase and frequency locked to the pump. By varying intracavity dispersion, we achieve a comb spanning 2.6–7.5 μm at a −20 dB level. Low pump threshold (down to 7 mW), high average power (up to 73 mW), broad spectral coverage, flat spectrum, and high coherence make this comb a source suitable for various applications, foremost dual-comb molecular spectroscopy.

OCIS codes: (190.4975) Parametric processes; (190.4410) Nonlinear optics, parametric processes; (320.7110) Ultrafast nonlinear optics.

http://dx.doi.org/10.1364/OL.41.001388

Broadband phase-stabilized frequency combs and, more generally, optical pulses with well-controlled electric fields in the mid-infrared (mid-IR; $\lambda > 2.5$ μm) region are imperative for a wide range of applications [1]. These include high-precision and high-sensitivity molecular spectroscopy, trace gas detection [2–4], dual-comb spectroscopy with massively parallel data collection [5–7], x-ray production via high harmonic generation [8], and laser-driven particle acceleration in microstructures [9]. Several techniques have been developed for producing mid-IR combs based on mode-locked lasers [6,10], optical rectification [5], difference-frequency generation [11–15], optical parametric oscillators [16,17], whispering gallery microresonators [18,19], and, most recently, quantum cascade lasers [20].

A method for broadband comb generation based on a divide-by-2 optical parametric oscillator (OPO) was demonstrated in [21,22]. A sync-pumped OPO operating at degeneracy rigorously both down-converts and augments the spectrum of a pump comb and manifests pulse compression in the time domain. This technique proved to be suitable for generating broadband combs in the mid-IR using periodically poled lithium niobate and orientation-patterned gallium arsenide (OP-GaAs) combined with different pump lasers. These include Er–fiber-laser-pumped (comb span 2.5–3.8 μm) [23], Cr^{2+}:ZnS-laser-pumped (span 3.6–5.6 μm) [24], and Tm–fiber-laser-pumped (span 2.6–6.1 μm) [25] subharmonic OPOs.

In a strictly degenerate OPO, the signal and idler waves are indistinguishable and the carrier envelope offset (CEO) frequency f_{CEO} is either half that of the pump, $f_{CEO,OPO} = f_{CEO,pump}/2$ (scenario A), or $f_{CEO,OPO} = f_{CEO,pump}/2 + f_{rep}/2$ (scenario B)—a consequence of three constraints imposed by (i) the fact that the OPO mode spacing is set by f_{rep}, the pulse repetition frequency of the pump, (ii) doubly resonant OPO operation, and (iii) photon energy conservation [22]. For a nondegenerate but still doubly resonant OPO, the signal and idler offsets are different, but nevertheless deterministic. The coherence properties of a doubly resonant femtosecond OPO were studied in detail for degenerate [26,27] and near-degenerate cases [28,29]. Subhertz relative linewidths between the pump and OPO comb teeth [29] and clean division of pump CEO frequency by 2 were experimentally demonstrated [27], thus proving that the OPO preserves coherence of the pump.

For simultaneous detection of molecules with different functional groups, one needs a spectrally broad comb, ideally spanning an octave or more. The instantaneous spans of well-characterized doubly resonant OPO combs were 3.3–5 μm [27], 3.1–3.5 μm, and 4.8–5.7 μm [29]. The broadest span achieved so far is 2.6–6.1 μm [25]; however, coherence properties were not assessed in that work and there were large (up to 30 dB) spectral density variations near the center of the spectrum. Here we report on an ultrabroadband 2.6–7.5 μm (at −20 dB) and uniform (less than 3 dB variation at 3.1–4.8 μm) frequency comb with up to 73 mW average power and prove its high coherence by measuring multiheterodyne beats in the RF domain.

The subharmonic OPO was synchronously pumped by an ultrafast Tm-fiber laser with a central wavelength of 1930 nm (FWHM 110 nm), repetition rate of 115 MHz, pulse duration of 90 fs, and average power of 330 mW. The Tm-fiber laser was a fully stabilized frequency comb: an octave-spanning 1100–2400 nm supercontinuum (SC) was generated in a highly nonlinear fiber and was used to phase lock the laser CEO frequency (by fast pump power modulation) to a stable RF synthesizer via f-to-$2f$ interferometry, while phase locking one of the SC comb lines relative to a 3-kHz-linewidth optical reference near 1564 nm via cavity length tuning, to stabilize the laser repetition rate f_{rep} [28,29]. The sync-pumped ring cavity OPO [Fig. 1(a)] was entirely composed of high-reflectivity gold-coated mirrors, except for one incoupling dielectric mirror (M1) with high transmission (>98%) around 1930 nm and high reflection (>90%) in the range 3.1–5.7 μm. On some occasions, the ring cavity was folded by adding one or two pairs of gold-coated mirrors to reduce its physical size. The nonlinear crystal was a 0.5-mm-long OP-GaAs with a 51.5 μm domain reversal period placed at a Brewster angle, similar to [25]. A 0.7-mm-thick wedged (1 deg) CaF_2 plate was used inside the cavity for (i) compensating and fine tuning the group delay dispersion and (ii) outcoupling the OPO power. The cavity was purged by dry air.

First we varied the OPO outcoupling from 0% to 52% by varying the Fresnel reflection of the CaF_2 wedge by turning the wedge away from the Brewster angle toward normal and then by rotating it in the orthogonal plane (s-plane), and measured the OPO pump threshold that varied from 7 mW (no outcoupling) to 279 mW (52% outcoupling). Because the OPO is doubly resonant, its pump threshold scales as the cavity loss squared, which was confirmed by the linear dependence in Fig. 1(b), where the vertical axis has a square-root scale. The mid-IR power (sum of two reflections from CaF_2 surfaces) versus outcoupling (sum of two surfaces) at the maximum pump (330 mW) is plotted in Fig. 1(c). At the optimal outcoupling of 22% we obtained 73 mW of average output mid-IR power with a slope efficiency of 40% and TEM_{00} mode. The measured pump depletion was 65%, while with no outcoupling it was as high as 90%. For the rest of the measurements discussed below, we chose an outcoupling of 5% (with 30 mW of output power).

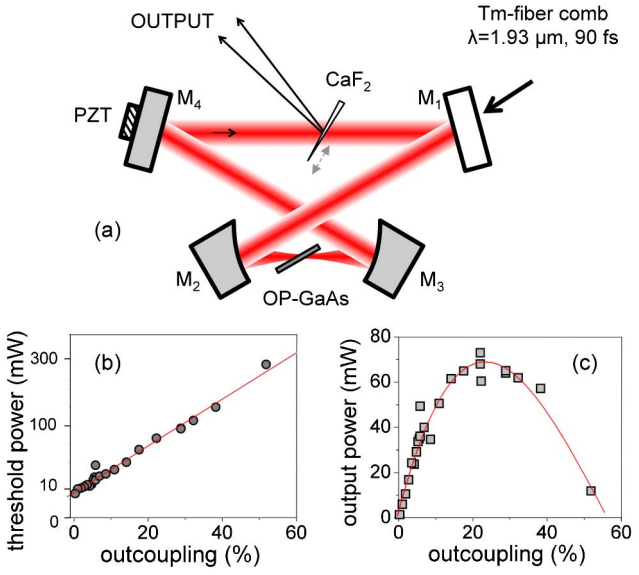

Fig. 1. (a) Schematic of the subharmonic OPO. Mirrors M2 and M3 are parabolic, with an off-axis angle of 30° and focal distance of 16 mm. PZT, piezoelectric actuator. (b) OPO pump threshold versus outcoupling. The solid line is a linear fit. Note that the y axis is plotted on a square-root scale. (c) OPO output power versus outcoupling at 330 mW pump. The solid curve is a trace for the eye.

We applied an active locking of the OPO cavity length using an electronic servo loop and a piezo actuator [PZT in Fig. 1(a)] [23,25]. Similar to [27], we observed (although to a lesser extent because of the much smaller average pump power) thermal self-locking of cavity-length resonances that allowed us to achieve stable OPO oscillation for up to several minutes. Thus in some occasions we operated the OPO without any active control. The OPO output spectra were measured with a Nicolet 6700 Fourier transform IR (FTIR) spectrometer.

The pump laser repetition rate f_{rep} was stabilized at 115.24 MHz (to about ±0.1 Hz), and the CEO frequency was locked at $f_{CEO,pump} = 40.48$ MHz. Similar to [27], to assess the CEO frequency of the OPO, we took advantage of the non-phase-matched sum frequency generation (SFG) in the GaAs crystal $\omega_{SFG} = \omega_{pump} + \omega_{OPO}$ in the range 1150–1450 nm. The SFG signal was separated from the main OPO output, fiber coupled, and combined, with an appropriate time delay, with the pump-generated SC. The RF beats were measured using a fast (350 MHz) balanced InGaAs photodetector and an RF spectrum analyzer, as shown in Fig. 2. The beat frequency between SFG and SC combs is given by $f_{RF} = (nf_{rep} + f_{CEO,pump} + f_{CEO,OPO}) - (mf_{rep} + f_{CEO,pump}) = (n-m)f_{rep} + f_{CEO,OPO}$, where n and m are integers. Hence f_{RF} is a measure of the OPO CEO frequency. For a degenerate OPO and scenario A, we expect the beat at $f_{RF} = f_{CEO,OPO} = f_{CEO,pump}/2 = 20.24$ MHz, while for scenario B, we expect the beat at $f_{CEO,OPO} = f_{CEO,pump}/2 + f_{rep}/2 = 77.86$ MHz, or rather its "mirror" image with respect to f_{rep} (115.24 - 77.86 = 37.38 MHz), since we used a low-pass (50 MHz) filter before the spectrum analyzer.

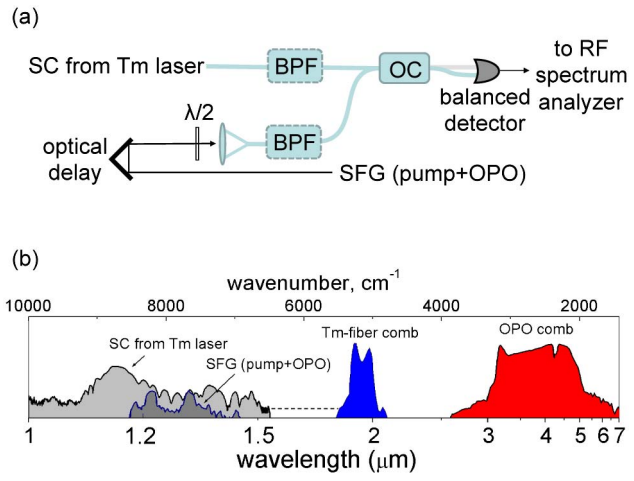

Fig. 2. (a) Setup for recording RF beats between the pump SC and parasitic SFG. BPF, fiber-based bandpass filter; OC, directional optical coupler. (b) Overview of the SC, SFG, Tm laser, and OPO spectra (log scale, arb. units). The dashed line shows the portion of the SC spectrum that was not measured.

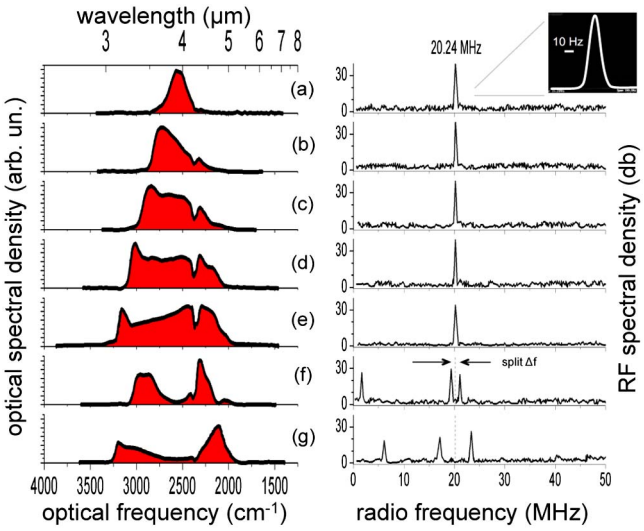

Fig. 3. Optical spectra (linear scale, left panel) and RF beats (log scale, right panel) at different thicknesses of the intracavity CaF_2, which was reduced by ~90 μm from (a) to (g). A dip near 2350 cm^{-1} (4.25 μm) is due to CO_2 in the air. The inset shows an RF peak obtained with high resolution.

First, by adjusting the optical delay [Fig. 2(a)], we obtained the beats between SC and SFG using fiber-based bandpass filters (BPFs; $\lambda_0 = 1220$ nm, FWHM 10 nm) in both channels. Then we removed the BPFs to allow collective heterodyne beats, characteristic of the whole OPO comb.

Due to the double resonance condition, the OPO oscillates at discrete values of the cavity length [22,23]. Switching to an adjacent length peak changes the CEO frequency by $f_{rep}/2$ [26]. In addition, switching to a neighboring peak changes, in a steplike fashion, the intracavity dispersion and hence the optical spectrum. For fine tuning dispersion and getting the broadest frequency comb, we translated the CaF_2 wedge to change its thickness around the optimal value of 0.7 mm and recorded the OPO spectra using an FTIR spectrometer. The spectra are shown on the left panel of Fig. 3, while the right panel displays corresponding RF spectra. From Figs. 3(a) to 3(g), the CaF_2 thickness was gradually reduced by ~90 μm (the free-space cavity length was accordingly adjusted to be at the same resonant peak). From Figs. 3(a) to 3(e), one can see that the CEO frequency stays at one-half that of the pump (20.24 MHz). The width of the RF peak was separately measured to be 15 Hz (Fig. 3, inset). This is an upper limit set by the resolution of our spectrum analyzer and is in accord with the results of [27], where a subhertz relative linewidth (with respect to the pump) was obtained.

By further varying intracavity dispersion [Figs. 3(f) and 3(g)], we detected a "phase" transition from a single-comb to a two-comb state: the optical spectrum manifested a pronounced two-humped structure, and the RF peak split symmetrically into two peaks spaced by $\Delta f = 1.75$ MHz [Fig. 3(f)] and 6.1 MHz [Fig. 3(g)]. This corresponds to two spectrally overlapping combs (signal and idler) with dissimilar CEO frequencies. Additionally, we detected low-frequency beats at Δf [Figs. 3(f) and 3(g)]. These beats were not sensitive to the delay between SC and SFG and occurred within the OPO spectrum itself. Moreover, when we directly recorded mid-IR output with a fast mercury cadmium telluride detector (VIGO System S.A.), we also observed, for the case of the scenarios in Figs. 3(f) and 3(g), the appearance of beats at frequency Δf.

When the OPO was switched to an adjacent cavity-length resonant peak, related to $f_{CEO,OPO} = f_{CEO,pump}/2 + f_{rep}/2$, we observed, as expected, an RF beat at 37.38 MHz. The evolution of the optical spectrum in Fig. 4 is the same as in Fig. 3, with the exception of a different CEO frequency. Similarly, we observed at some point the fragmenting into two combs with f_{CEO} split by $\Delta f = 2$ MHz [Fig. 4(f)] and 6.5 MHz [Fig. 4(g)].

Figure 5 shows the broadest spectrum that we achieved in a coherent single-comb OPO mode. The instantaneous comb span reached 2.6–7.5 μm ($\Delta\nu = 2513$ cm^{-1}, 1.53 octaves) at a −20 dB level and 3.13–4.75 μm (1090 cm^{-1}, 0.6 octaves) at a −3 dB level. The dashed curve in Fig. 5 is the residual phase

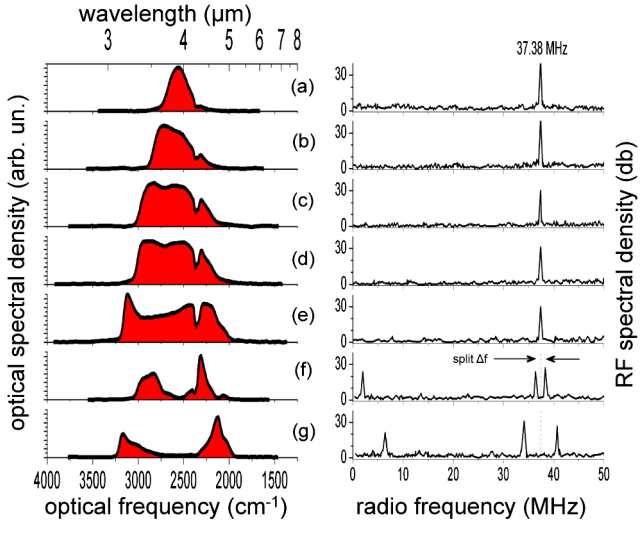

Fig. 4. Same as Fig. 3, but for the adjacent cavity-length peak. The thickness of the CaF_2 is reduced by ~90 μm from (a) to (g).

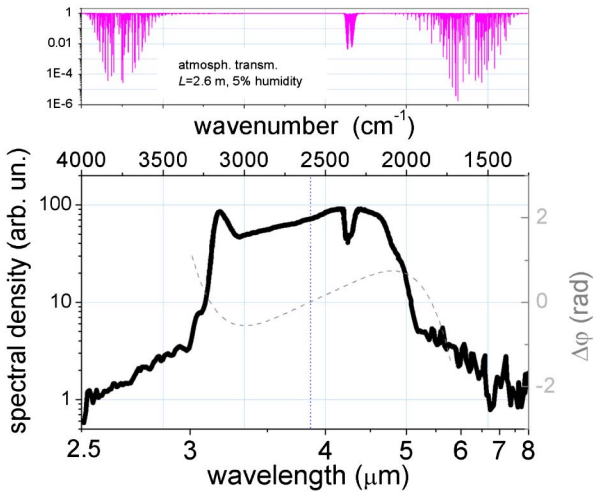

Fig. 5. Frequency comb spectrum measured with an FTIR spectrometer. The spectral span is 2.6–7.5 μm at the −20 dB level. The vertical dotted line is the OPO degeneracy (3.86 μm). The dashed line is an accumulated extra phase per round trip. The top panel shows the simulated transmission through 2.6 m (cavity round-trip length) of the purged (5% humidity) air.

delay per round trip corresponding to this case, calculated from the contribution of GaAs, CaF_2, and mirror M1.

Also shown (top part of Fig. 5) is a simulated transmission (HITRAN database) through 2.6 m (cavity length) of the purged (5% humidity) atmosphere. The absorption near 3750 and 1500 cm^{-1} is due to residual water vapor, and near 2350 cm^{-1} it is due to CO_2 in the air. Better cavity purging (e.g., using dry nitrogen versus dry air) will eliminate these dips (especially CO_2 dip) that influence not only absorption but also dispersion of the cavity.

In summary, we produced a frequency comb with an instantaneous wavelength span of 2.6–7.5 μm, and studied its coherence by observing RF multiheterodyne beats between the SC originating from the pump and SFG from the OPO. To the best of our knowledge, it is the broadest (in frequency units) frequency comb in the mid-IR. The combination of a flat broadband spectrum, high power, and high coherence in the spectral region of fundamental molecular vibrations makes the comb interesting in the rapidly progressing field of trace gas sensing.

Funding. Office of Naval Research (ONR) (N00014-15-1-2659); Defense Advanced Research Projects Agency (DARPA) (W31P4Q-15-1-0008).

Acknowledgment. We thank Nathaniel Lee and Jia Xu for their help in performing experiments, and Kevin Lee for sharing his expertise in RF beat measurements.

REFERENCES

1. A. Schliesser, N. Picqué, and T. W. Hänsch, Nat. Photonics **6**, 440 (2012).
2. D. Mazzotti, P. Cancio, G. Giusfredi, P. De Natale, and M. Prevedelli, Opt. Lett. **30**, 997 (2005).
3. F. Adler, P. Masłowski, A. Foltynowicz, K. C. Cossel, T. C. Briles, I. Hartl, and J. Ye, Opt. Express **18**, 21861 (2010).
4. L. Nugent-Glandorf, T. Neely, F. Adler, A. J. Fleisher, K. C. Cossel, B. Bjork, T. Dinneen, J. Ye, and S. A. Diddams, Opt. Lett. **37**, 3285 (2012).
5. F. Keilmann, C. Gohle, and R. Holzwarth, Opt. Lett. **29**, 1542 (2004).
6. B. Bernhardt, E. Sorokin, P. Jacquet, R. Thon, T. Becker, I. T. Sorokina, N. Picqué, and T. W. Hänsch, Appl. Phys. B **100**, 3 (2010).
7. Y. W. Jin, S. M. Cristescu, F. J. M. Harren, and J. Mandon, Appl. Phys. B **119**, 65 (2015).
8. P. B. Corkum and F. Krausz, Nat. Phys. **3**, 381 (2007).
9. E. A. Peralta, K. Soong, R. J. England, E. R. Colby, Z. Wu, B. Montazeri, C. McGuinness, J. McNeur, K. J. Leedle, D. Walz, E. B. Sozer, B. Cowan, B. Schwartz, G. Travish, and R. L. Byer, Nature **503**, 91 (2013).
10. C.-C. Lee, C. Mohr, J. Bethge, S. Suzuki, M. E. Fermann, I. Hartl, and T. R. Schibli, Opt. Lett. **37**, 3084 (2012).
11. C. Erny, K. Moutzouris, J. Biegert, D. Kühlke, F. Adler, A. Leitenstorfer, and U. Keller, Opt. Lett. **32**, 1138 (2007).
12. A. Gambetta, R. Ramponi, and M. Marangoni, Opt. Lett. **33**, 2671 (2008).
13. P. Malara, P. Maddaloni, G. Gagliardi, and P. De Natale, Opt. Express **16**, 8242 (2008).
14. D. Sánchez, M. Hemmer, M. Baudisch, K. Zawilski, P. Schunemann, H. Hoogland, R. Holzwarth, and J. Biegert, Opt. Lett. **39**, 6883 (2014).
15. F. C. Cruz, D. L. Maser, T. Johnson, G. Ycas, A. Klose, F. R. Giorgetta, I. Coddington, and S. A. Diddams, Opt. Express **23**, 26814 (2015).
16. J. H. Sun, B. J. S. Gale, and D. T. Reid, Opt. Lett. **32**, 1414 (2007).
17. F. Adler, K. C. Cossel, M. J. Thorpe, I. Hartl, M. E. Fermann, and J. Ye, Opt. Lett. **34**, 1330 (2009).
18. C. Y. Wang, T. Herr, P. Del'Haye, A. Schliesser, J. Hofer, R. Holzwarth, T. W. Hänsch, N. Picqué, and T. J. Kippenberg, Nat. Commun. **4**, 1345 (2013).
19. A. G. Griffith, R. K. W. Lau, J. Cardenas, Y. Okawachi, A. Mohanty, R. Fain, Y. H. D. Lee, M. Yu, C. T. Phare, C. B. Poitras, A. L. Gaeta, and M. Lipson, Nat. Commun. **6**, 6299 (2015).
20. A. Hugi, G. Villares, S. Blaser, H. C. Liu, and J. Faist, Nature **492**, 229 (2012).
21. S. T. Wong, T. Plettner, K. L. Vodopyanov, K. Urbanek, M. Digonnet, and R. L. Byer, Opt. Lett. **33**, 1896 (2008).
22. S. T. Wong, K. L. Vodopyanov, and R. L. Byer, J. Opt. Soc. Am. B **27**, 876 (2010).
23. N. Leindecker, A. Marandi, R. L. Byer, and K. L. Vodopyanov, Opt. Express **19**, 6296 (2011).
24. V. O. Smolski, S. Vasilyev, P. G. Schunemann, S. B. Mirov, and K. L. Vodopyanov, Opt. Lett. **40**, 2906 (2015).
25. N. Leindecker, A. Marandi, R. L. Byer, K. L. Vodopyanov, J. Jiang, I. Hartl, M. Fermann, and P. G. Schunemann, Opt. Express **20**, 7046 (2012).
26. A. Marandi, N. Leindecker, V. Pervak, R. L. Byer, and K. L. Vodopyanov, Opt. Express **20**, 7255 (2012).
27. K. F. Lee, C. Mohr, J. Jiang, P. G. Schunemann, K. L. Vodopyanov, and M. E. Fermann, Opt. Express **23**, 26596 (2015).
28. K. F. Lee, J. Jiang, C. Mohr, J. Bethge, M. E. Fermann, N. Leindecker, K. L. Vodopyanov, P. G. Schunemann, and I. Hartl, Opt. Lett. **38**, 1191 (2013).
29. K. F. Lee, N. Granzow, M. A. Schmidt, W. Chang, L. Wang, Q. Coulombier, J. Troles, N. Leindecker, K. L. Vodopyanov, P. G. Schunemann, M. E. Fermann, P. St.J. Russell, and I. Hartl, Opt. Lett. **39**, 2056 (2014).